2018

Molecular Determinants Conferring the Stoichiometric-Dependent Activity of α-Conotoxins at the Human α9α10 Nicotinic Acetylcholine Receptor Subtype

Rilei Yu
Qingdao National Laboratory for Marine Science and Technology, Ocean University of China

Han-Shen Tae
University of Wollongong

Nargis Tabassum
Ocean University of China, Qingdao National Laboratory for Marine Science and Technology

Juan Shi
Ocean University of China, Qingdao National Laboratory for Marine Science and Technology

Tao Jiang
Qingdao National Laboratory for Marine Science and Technology, Ocean University of China

See next page for additional authors

Publication Details

Yu, R., Tae, H., Tabassum, N., Shi, J., Jiang, T. & Adams, D. J. (2018). Molecular Determinants Conferring the Stoichiometric-Dependent Activity of α-Conotoxins at the Human α9α10 Nicotinic Acetylcholine Receptor Subtype. Journal of Medicinal Chemistry, 61 (10), 4628-4634.

Molecular Determinants Conferring the Stoichiometric-Dependent Activity of α-Conotoxins at the Human α9α10 Nicotinic Acetylcholine Receptor Subtype

Abstract
α9α10 nicotinic acetylcholine receptors (nAChRs) putatively exist at different stoichiometries. We systematically investigated the molecular determinants of α-conotoxins Vc1.1, RgIA#, and PeIA inhibition at hypothetical stoichiometries of the human α9α10 nAChR. Our results suggest that only Vc1.1 exhibits stoichiometric-dependent inhibition at the α9α10 nAChR. The hydrogen bond between N154 of α9 and D11 of Vc1.1 at the α9(+)-α9(−) interface is responsible for the stoichiometric dependent potency of Vc1.1.

Disciplines
Medicine and Health Sciences

Publication Details
Yu, R., Tae, H., Tabassum, N., Shi, J., Jiang, T. & Adams, D. J. (2018). Molecular Determinants Conferring the Stoichiometric-Dependent Activity of α-Conotoxins at the Human α9α10 Nicotinic Acetylcholine Receptor Subtype. Journal of Medicinal Chemistry, 61 (10), 4628-4634.

Authors
Rilei Yu, Han-Shen Tae, Nargis Tabassum, Juan Shi, Tao Jiang, and David J. Adams

Molecular determinants conferring the stoichiometric-dependent activity of α-conotoxins at the human α9α10 nAChR subtype

Rilei Yu[1,3†*], Han-Shen Tae[2†], Nargis Tabassum[1,3], Juan Shi [1,3], Tao Jiang[1,3] and David J. Adams[2*]

[1]*Key Laboratory of Marine Drugs, Chinese Ministry of Education, School of Medicine and Pharmacy, Ocean University of China, Qingdao 266003, China*

[2]*Illawarra Health and Medical Research Institute (IHMRI), University of Wollongong, Wollongong, New South Wales 2522, Australia*

[3]*Laboratory for Marine Drugs and Bioproducts of Qingdao National Laboratory for Marine Science and Technology, Qingdao 266003, China*

[†]These authors contribute equally to this work.

[*]Corresponding authors: djadams@uow.edu.au or ryu@ouc.edu.cn

ABSTRACT

α9α10 Nicotinic acetylcholine receptors (nAChRs) putatively exist at different stoichiometries. We systematically investigated the molecular determinants of α-conotoxins Vc1.1, RgIA#, and PeIA inhibition at hypothetical stoichiometries of the human α9α10 nAChR. Our results suggest that only Vc1.1 exhibits strong stoichiometric-dependent inhibition at the α9α10 nAChR. The hydrogen bond between N154 of α9 and D11 of Vc1.1 at the α9(+)-α9(−) interface is responsible for the stoichiometric-dependent potency of Vc1.1.

Introduction

Nicotinic acetylcholine receptors (nAChRs) are cation-selective pentameric ligand-gated ion channels belonging to the family of Cys-loop receptors, which also includes γ-aminobutyric acid type A ($GABA_A$), glycine, and serotonin ($5\text{-}HT_3$) receptors.[1] The vertebrate nAChRs are homo/heteromeric assembles of α1-α10, β1-β4, γ, δ or ε subunits. Although the nAChRs are generally featured in the nervous system, they are also expressed in non-neuronal cells participating in various physiological events and they are important targets for drug design.[2]

The first crystal structure of any heteromeric nAChRs, the human(h) α4β2 nAChR subtype, reveals the overall architecture consisting of a large extracellular domain (ECD), a transmembrane domain (TMD) and an intracellular domain (ICD) (Figure 1A).[3] The ligand binding site is located at the ECD interface of two adjacent subunits, comprising of (+) (principal) and (−) (complementary) components. For hα4β2 nAChR, the α4 subunit loops A, B and C form the (+) site, and the β2 subunit β-sheet contributes to the (−) site (Figure 1B). Five subunits of the nAChR circle a conducting pore (Figure 1C) where a gate consisting of hydrophobic residues, such as Leu and Ile, is located in the middle of the TMD.

Heteromeric α9α10 nAChRs play an important physiological role in mediating olivocochlear and vestibular neurotransmission.[4,5] Transcripts/protein expression of α9 and/or α10 subunits have been reported in dorsal root ganglion neurons,[6,7] adrenal medulla,[8] and in other non-neuronal cells, such as skin keratinocytes, pituitary pars tuberalis, lymphocytes, macrophages and bladder urothelium.[9–15]

α9-Containing nAChRs are potential targets for the therapy of several disorders or diseases such as ear disorders, chronic pain and pemphigus vulgaris.[7,9,11,16,17] In addition, α9-containing nAChRs are responsible for nicotine-induced transformation of normal human breast epithelial cells, and inducible overexpression of α9-nAChR substantially increased tumor growth.[18]

Conotoxins derived from the venom of *Conus* sea snails are pharmacologically valuable peptides with selective potency at nAChR subtypes. α-Conotoxin antagonists of α9α10 nAChR such

as *C. victoriae* Vc1.1, *C. regius* RgIA (Figure 2), and *C. generalis* GeXIVA are short and well-folded peptides with analgesic effect in rat models of neuropathic pain.[19,20] In addition, PeIA from *C. pergrandis*, displays high selectivity for the α9α10 nAChR subtype.[21] Similar to Vc1.1 and RgIA, PeIA is also a potent inhibitor of N-type calcium channels via $GABA_B$ receptor activation.[22]

Despite their specificity at inhibiting α9α10 nAChRs, the binding site and the stoichiometry-dependent sensitivity of each α-conotoxin are varied. The stoichiometry of rat(r) α9α10 nAChR heterologously expressed in *Xenopus laevis* oocytes was initially suggested to consist of two α9 and three α10 subunits ($(\alpha9)_2(\alpha10)_3$).[23] Based on this stoichiometry, Vc1.1 was postulated to bind preferentially at the α10(+)-α9(—) interface.[24] However, Indurthi *et al*. proposed at least two stoichiometries (see Figure 1D,E), possibly $(\alpha9)_2(\alpha10)_3$ and $(\alpha9)_3(\alpha10)_2$, with a high Vc1.1-sensitive α9(+)-α9(—) binding site present in the $(\alpha9)_3(\alpha10)_2$ composition, and two low Vc1.1-sensitive binding sites contributed by the α10(+)-α9(—) and/or α9(+)-α10(—) interfaces that are common in both subunit arrangements.[25] In contrast, RgIA exhibited no preference for the Vc1.1-high sensitivity binding site of the α9α10 nAChR, and it was reported that RgIA has a high affinity for the α10(+)-α9(—) interface.[26]

The molecular determinants that govern the binding site selectivity and stoichiometry-dependent sensitivity of Vc1.1, RgIA, and PeIA at α9α10 nAChR, however, remain elusive and the activity of PeIA at different α9α10 nAChR stoichiometries is yet to be reported. In this study, we performed comprehensive computational modeling based on the proposed high and low Vc1.1 sensitivity binding sites in $(\alpha9)_2(\alpha10)_3$ and $(\alpha9)_3(\alpha10)_2$ stoichiometries, in combination with mutagenesis study on hα9α10 nAChRs expressed in oocytes injected with varied α9:α10 mRNA ratios. The sequences of Vc1.1, RgIA, and PeIA are remarkably different from each other despite their relatively potent antagonism of the α9α10 nAChR. We aim to identify residues of the receptor and/or peptides responsible for the α9α10 nAChR binding site selectivity and sensitivity of these peptides. This information is essential for the design of α-conotoxin analogues with improved selectivity for a specific α9α10 nAChR stoichiometry.

Results and discussion

Molecular dynamics simulations

Vc1.1 was postulated to inhibit α9α10 nAChR by binding at a high affinity α9(+)-α9(—) interface and/or a low affinity α10(+)-α9(—) interface.[24,25] Both Vc1.1 binding sites share a common α9 subunit (—) component, therefore, the determinants of Vc1.1 binding should be contributed by non-conserved residues of the α9 and α10 subunit (+) components. Overall, our molecular dynamics (MD) simulation model suggests, the binding modes of Vc1.1 at both α9(+)-α9(—) and α10(+)-α9(—) interfaces are similar with four salt-bridges formed involving charged residues of Vc1.1 (R7, D11, H12 and E14) and conserved residues of the hα9 and hα10 subunits (R81, R113, E197 and D201). The R7-D201, H12-E197, D11-R81 and E14-R113 hydrogen bonds (Figure 3A,B) are consistent with the previously proposed interaction of Vc1.1 with the α10 subunit (+) site residues.[24]

In addition to the interaction with R81 of the α9 subunit (—) component, D11 of Vc1.1 forms additional hydrogen bond with a non-conserved N154 at the α9(+)-α9(—) interface (Figure 3B). In comparison, the corresponding α10 subunit residue G154 (Figure 3A) is incapable of direct interaction with Vc1.1. Other non-conserved α9 and α10 subunit (+) site residues at position 188 and 190 are postulated to have no contribution to the binding affinity of Vc1.1. Our model postulates residues α9 N188 and α10 R188 are not feasibly located to interact with Vc1.1, whereas residues α9 I190 and α10 L190 have similar side chains.

In this study, we used the R13-deleted analogue of RgIA (RgIA#) to probe its sensitivity to different stoichiometries of α9α10 nAChRs. RgIA# has been reported to have comparable activity to the wild-type RgIA.[27,28] RgIA# has an internal salt-bridge formed between residues D5 and R7, involved in binding at both α10(+)-α9(–) and to α9(+)-α9(–) interfaces. At both binding sites, residues R7 and R9 of RgIA# are buried in the binding pockets forming salt-bridges with D201 and D121 of the (+) and (–) components, respectively (Figure 3C,D). Similarly, the conserved aspartate residues D201 and D121 were suggested to interact with RgIA residues R7 and R9, respectively, at the rα10(+)-α9(–) interface.[28] It was also proposed that R11 of RgIA interacts with E197 of the rα10

subunit. However, residue R11 of RgIA# is solvent exposed and flexible in our MD simulations, and only occasionally approaching E197 of the α10 and α9 (+) components forming unstable salt-bridges.

The DPR (Asp-Pro-Arg) motif is conserved in α-conotoxins ImI, RgIA# (or RgIA) and Vc1.1, and essential to their binding affinities.[26,29–31] However, this sequence epitope is not present in PeIA despite its higher potency at inhibiting the hα9α10 nAChR than Vc1.1 and RgIA# (Figure 2, S1). In PeIA, the side chain of H5 forms an internal hydrogen bond with C8 (Figure S2), which might be essential to stabilize the secondary structure of the peptide. No remarkable differences were observed in the binding of PeIA at the α10(+)-α9(—) and α9(+)-α9(—) interfaces. Similar to Vc1.1, PeIA residues H12 and E14 interact with residues E197 of the (+) and R113 of the (—) components, respectively (Figure 3E,F).

In contrast to Vc1.1, both RgIA# and PeIA do not interact with N154 of the α9 subunit (+) component and for PeIA, an additional hydrogen bond is formed between residue N11 (D11 in Vc1.1) and T152 of the (+) component at both binding sites. Therefore, our model suggests lack of binding site preference between α10(+)-α9(—) and α9(+)-α9(—) for RgIA# and PeIA.

Energy calculations

Quantitative evaluation on the contribution of the principal site residues to Vc1.1, RgIA# and PeIA binding affinity was assessed using the MMGB/SA (molecular mechanics generalized Born/surface area) method (Figure S3). Conserved residues on both α9 and α10 subunit (+) sites such as Y95, W151, T152, Y192, C194, C195, E197 and Y199 significantly contribute to the binding affinity of Vc1.1, RgIA# and PeIA. Indeed, in our model the aromatic residues of the binding site form compact van der Waals contacts with the α-helix of the α-conotoxins, and the C192-C193 disulfide bond stacks with the C2-C8 disulfide bond of the α-conotoxins. However, for the four (+) site non-conserved residues at positions 154, 188, 190 and 191, only residue 154 (N in α9 subunit and G in α10 subunit) showed significant difference in the binding energy upon interaction with Vc1.1 (Figure S3 A). The side chain of α9 N154 contributes about –4 kcal/mol, whereas α10 G154 only

resulted in –0.19 kcal/mol Vc1.1-binding energy shift. Binding energy calculations for RgIA# (Figure S3B) and PeIA (Figure S3C) showed minor contribution of α9 N154 and α10 G154 in the interactions with both α-conotoxins.

RgIA was suggested to have a high affinity binding site at the rat α10(+)-α9(–) interface based on the stoichiometry model of $(\alpha9)_2(\alpha10)_3$ nAChR.[26] Our modeling studies showed comparable RgIA# binding energy at the principal subunits of α9(+) and α10(+) hence suggesting RgIA# has no binding preference for either α9(+)-α9(–) or α10(+)-α9(–) interfaces of the $(\alpha9)_3(\alpha10)_2$ nAChR.

Overall, our computational studies suggest Vc1.1 possesses binding preference for the α9(+)-α9(—) interface than the α10(+)α9(—) interface. Binding of RgIA# and PeIA at the hα9α10 nAChR on the other hand, is less dependent on the stoichiometry. A hydrogen-bond is formed between α9 N154 and Vc1.1 D11 at the α9(+)-α9(—) interface and most importantly, this interaction is absent in RgIA# and PeIA binding models at the aforementioned hα9α10 nAChR site.

Electrophysiology

Injection of biased α9 to α10 subunit mRNA ratios resulted in putative $(\alpha9)_3(\alpha10)_2$ and $(\alpha9)_2(\alpha10)_3$ stoichiometries of the rα9α10 nAChRs heterologously expressed in *X. laevis* oocytes.[25] Consequently, a high-sensitivity Vc1.1 binding site was proposed at the α9(+)-α9(–) interface present only in the $(\alpha9)_3(\alpha10)_2$ stoichiometry, and a low–sensitivity Vc1.1 binding site contributed by the α10(+)-α9(–) interface that exists in both stoichiometries. Most importantly, the stoichiometry of the rα9α10 nAChR expressed at 1:1 (or 10:1) and 1:3 ratios of α9:α10 mRNA was proposed to be $(\alpha9)_3(\alpha10)_2/(\alpha9)_4(\alpha10)_1$ and $(\alpha9)_2(\alpha10)_3$ nAChRs, respectively.

To validate our prediction that the hydrogen bond interaction between Vc1.1 D11-α9 and N154 is the determinant of Vc1.1 binding preference at the hα9(+)-α9(–) interface, residue N154 of the hα9 subunit was mutated to the corresponding hα10 subunit G154. We determined the biological activity of Vc1.1, RgIA#, PeIA and, analogues Vc1.1[D11N] and Vc1.1[PeIA] at heterologously co-expressed hα9/α9[N154G] and α10 subunits in *X. laevis* oocytes, injected at varying mRNA ratios.

Concentration-response relationships for Vc1.1, RgIA# and PeIA inhibition of hα9α10 nAChR, expressed from an α9:α10 mRNA ratio of 1:1, gave half-maximal inhibitory concentration (IC_{50}) values of 1.0 ± 0.1 μM (n = 10-16), 248.7 ± 19.2 nM (n = 5-6) and 22.2 ± 1.6 nM (n = 6-8), respectively (Figure S1). Subsequent experiments were carried out using 1 μM Vc1.1, 300 nM RgIA# and 30 nM PeIA, close to the IC_{50} values of the α-conotoxins at the hα9α10 nAChR.

At α9:α10 mRNA ratios of 3:1 putatively resulting in $(\alpha9)_3(\alpha10)_2$ and/or $(\alpha9)_4(\alpha10)_1$ nAChRs, 1 μM Vc1.1 inhibited ACh-evoked currents by 65.8 ± 1.8% (n = 16), respectively (Figure 4A). However, at α9:α10 mRNA ratio of 1:3, presumably forming the $(\alpha9)_2(\alpha10)_3$ nAChR stoichiometry, 1 μM Vc1.1 inhibited ACh-evoked currents by 25.5 ± 1.8% (n = 15). Similarly, Vc1.1 antagonized only ~20% of the ACh-evoked currents mediated by α9[N154G]α10 nAChRs at 1:3 (19.5 ± 1.0%, n = 12) and 3:1 (21.8 ± 2.2%, n = 14) α9:α10 mRNA ratios (Figure 4A).

Vc1.1 concentration-response relationships for hα9α10 nAChRs expressed from biased α9:α10 ratios revealed IC_{50} values of 0.75 μM at 3:1 ratio compared to 3.57 μM for 1:3 ratio (Figure S3, Table 1). N154G mutation to the hα9 subunit, however, reduced the potency of Vc1.1 with IC_{50}'s of 11.25 μM and 17.02 μM for hα9[N154G]α10 nAChRs at 1:3 and 3:1 ratios, respectively. Injections of higher α9 to α10 mRNA ratios resulted in greater Vc1.1 inhibition at the expressed hα9α10 nAChRs compared to injections with excess α10 mRNA, alluding to the presence of Vc1.1-high sensitivity α9(+)-α9(–) site/s in the $(\alpha9)_3(\alpha10)_2$ or $(\alpha9)_4(\alpha10)_1$ configurations. By contrast, α9[N154G]α10 nAChRs expressed from α9[N154G]:α10 ratios of 1:3 or 3:1 showed similar sensitivity to Vc1.1 inhibition. However, compared to the wild-type receptors, the potency of Vc1.1 inhibition at α9[N154G]α10 nAChRs expressed from α9:α10 mRNA injection at ratios of 3:1 was decreased ~23-fold whereas at 1:3 mRNA ratio the potency of Vc1.1 was reduced 3-fold. Although the α9 subunit (+) component N154 residue is postulated to be critical for Vc1.1 high affinity binding at the α9(+)-α9(–) interface, it should be noted that despite the lack of such interface at the 1:3 ratio, Vc1.1 inhibition is affected. The 3-fold reduction of Vc1.1 potency might be explained either by the conformational effects of the mutation to the α10(+)α9(—) binding site or by the

removal of the α9 N154 at the α9(+)α10(—) binding site.

In contrast to Vc1.1, varying the α9:α10 mRNA ratios resulted in minor sensitivity differences of both α9α10 and α9[N154G]α10 nAChRs to RgIA# or PeIA inhibition (Figure 4B,C). The α9[N154G] substitution only slightly affected the sensitivity of the mutant receptors to inhibition by both peptides. In our model, the side chain of N154 is not located in close proximity to either PeIA or RgIA#, which may explain their minimal sensitivity difference to either interfaces of α9(+)-α9(—) or α10(+)-α9(—) formed at the different α9α10 nAChR stoichiometries. Previous mutagenesis studies suggested that the most favourable binding site of RgIA is at the α10(+)α9(—) interface of $r(\alpha9)_2(\alpha10)_3$ nAChR.[26] Similar to RgIA#, PeIA showed no stoichiometric-dependent inhibition of hα9α10 nAChRs, suggesting that both peptides showed no preferable binding to α9(+)-α9(—) versus α10(+)-α9(—)/α9(+)-α10(—).

Vc1.1[D11N] exhibited significantly lower potency than wild-type Vc1.1 at hα9α10 nAChRs at both 1:3 and 3:1 ratios with IC_{50} values of 17.54 μM (5-fold decrease) and 10.79 μM (14-fold decrease), respectively (Table 1). On the other hand, at α9[N154G]α10 nAChRs, Vc1.1[D11N] and Vc1.1 possess comparable inhibitory activity at both ratios. The substantially reduced inhibitory activity of Vc1.1[D11N] compared to the wild-type Vc1.1 might be due to the removal of R81-D11 charge interaction at both α9(+)α9(—) and α10(+)α9(—) interfaces as well as disruption to the hydrogen bond between N154 and D11 at the α9(+)α9(—) interface (Figure 3A,B). Using thermodynamic mutant cycles,[32] the coupling coefficient (Ω) gave a reciprocal of 28.57 suggesting a relatively strong coupling between Vc1.1 D11 and α9 N154 . Additionally, the coupling energy between Vc1.1 D11 and α9 N154 was calculated to be 1.95 kcal/mol, comparable to the hydrogen bond energy between N-H and O (~1.9 kcal/mol),[33] further demonstrating the key pairwise interaction between Vc1.1 D11 and α9 N154.

Vc1.1[PeIA] analogue has residues S9–L15 of PeIA grafted to the corresponding region of Vc1.1 (Figure 2) and similar to Vc1.1[D11N], Vc1.1[PeIA] has an asparagine residue at position 11. Vc1.1[PeIA] exhibited a similar degree of inhibition at both hα9α10 and hα9[N154G]α10 nAChRs

expressed from mRNA injection ratios of 1:3 and 3:1. Similar to Vc1.1[D11N], Vc1.1[PeIA] had reduced inhibitory activity at hα9α10 nAChRs compared to Vc1.1 with the potency decreased ~4 fold and ~12-fold at 1:3 and 3:1 ratios, respectively. Thus, PeIA second loop grafting to Vc1.1 resulted in a greater decrease in potency at the hα9α10 nAChR expressed from high α9:α10 mRNA ratio. Furthermore, Vc1.1[PeIA] and Vc1.1 possess comparable IC_{50} at hα9[N154G]α10 nAChR (at 1:3 and 3:1 ratios). The insensitivity of Vc1.1[PeIA] to α9α10 or α9[N154G]α10 nAChRs expressed with excess α9 (or α9[N154G]) or α10 mRNAs resulted from the replacement of the residues, especially D11 at the second loop of Vc1.1. As shown in PeIA-α9(+)α9(—) model (Figure 3F), residues from the second loop of PeIA form few contacts with the side chain of α9 N154. Thus, similar to Vc1.1[D11N], Vc1.1[PeIA] shows minor activity differences between hα9α10 nAChRs expressed from mRNA injection ratios of 1:3 and 3:1.

The decreased binding affinity of Vc1.1[D11N] and Vc1.1[PeIA] at the α9α10 nAChRs from 1:3, and 3:1 mRNA ratios is unlikely due to the peptide conformational changes. In MD simulations, the backbone RMSD for Vc1.1[D11N] and Vc1.1[PeIA] are comparable to Vc1.1 suggesting that the conformation of both Vc1.1 analogues is similar to the wild-type peptide (Figure S5). In addition, the circular dichroism profiles of Vc1.1[D11N] and Vc1.1[PeIA] were similar to the wild-type peptides, Vc1.1 and PeIA, further suggesting that sequence mutations and sequence replacement resulted in minimal conformation perturbation (Figure S6).

Conclusion

Our computational modelling in combination with mutagenesis studies support that the stoichiometry of the hα9α10 nAChR expressed with α9:α10 mRNA injection ratios of 1:3 and 3:1 could correspond to $(\alpha9)_2(\alpha10)_3$ and $(\alpha9)_3(\alpha10)_2/(\alpha9)_4(\alpha10)_1$ nAChRs, respectively. The $(\alpha9)_3(\alpha10)_2/(\alpha9)_4(\alpha10)_1$ nAChR arrangement uniquely contains an α9(+)-α9(—) interface binding site that is responsible for the higher sensitivity of the receptor to Vc1.1 than that of the $(\alpha9)_2(\alpha10)_3$ nAChR. The non-conserved residue at position 154 of both hα9 and hα10 subunits essentially differentiates the binding affinity of Vc1.1 to α9(+)-α9(—) and α10(+)-α9(—) interfaces. The

hydrogen bond formed between the side chains of α9 N154 and Vc1.1 D11 confers the specificity of Vc1.1 at α9(+)-α9(—) interface, and is responsible for the higher sensitivity of the α9α10 nAChR expressed with higher abundance of the α9 mRNA to Vc1.1. The α10(+)-α9(—) interface is the most favourable Vc1.1 binding site at $(\alpha9)_2(\alpha10)_3$ nAChR whereas at $(\alpha9)_3(\alpha10)_2$/$(\alpha9)_4(\alpha10)_1$ nAChR, the interface of α9(+)-α9(—) rather than α10(+)-α9(—) interface has higher affinity for Vc1.1. Despite sharing the same disulfide-bond framework with Vc1.1, PeIA demonstrates no obvious stoichiometry-dependent inhibition of α9α10 nAChRs and it also does not discriminate between either α9(+)-α9(—) or α10(+)-α9(—) interfaces from our modelling studies. RgIA# exhibits no preferential inhibitory activity at either $(\alpha9)_3(\alpha10)_2$ or $(\alpha9)_2(\alpha10)_3$ nAChRs and residues of RgIA# have no remarkable specific pairwise interactions to the interfaces of α9(+)-α9(—) or α10(+)-α9(—). However, we cannot exclude the possibility of the α9(+)-α9(—) as an energetically favourable binding site of RgIA# at $(\alpha9)_3(\alpha10)_2$ nAChR. Instead, our study suggests that the sensitivity of both α10(+)-α9(—) and α9(+)-α9(—) interfaces to RgIA# might be comparable. In a previous study, the contribution of α9 and α10 subunits to complementary components of the ligand-binding site was proposed to be non-equivalent,[34] whereas we found the contribution of α9 and α10 subunits to principal components of the ligand-binding site was non-equivalent for Vc1.1 binding but could be equivalent for the binding of RgIA# and PeIA.

In summary, elucidation of the determinants that confer the selectivity of the α-conotoxins to varied subunit arrangements of the hα9α10 nAChR is essential for rational design of novel stoichiometric-selective α-conotoxin analogues. Whether different stoichiometries of hα9α10 nAChR exist *in vivo* is yet to be determined. Regardless, stoichiometric-selective inhibitors of α9α10 nAChR would be useful neurochemical tools for further elucidating the functional differences between the stoichiometries in native cells. Conversely, α9α10 nAChR antagonists that do not discriminate between the stoichiometries, may be suitable candidates to use under conditions where different stoichiometries exist.

Methods

Homology modeling

Models of Vc1.1 bound h$(\alpha9)_2(\alpha10)_3$ and h$(\alpha9)_2(\alpha10)_3$ nAChRs were built using Modeller (version 9v14), as described previously.[24,30] The extracellular domain sequence of the hα1, α3, α4, α6, α7, α9, and α10 nAChR subunits were retrieved from the Uniprot database.[35] Both crystal structures of *Aplysia californica* AChBP (acetylcholine binding protein) in complex with α-conotoxin PnIA[A10L,D14K] (PDB code 2BR8), and the hα9 nAChR subunit extracellular domain (PDB code 4D01) from the Protein Data Bank, were used as templates to build 200 models of each α-conotoxin-nAChR complexes.[36,37] Models with the lowest DOPE score were selected for further structural refinement using molecular dynamics (MD) simulations. The structures of Vc1.1 analogues, Vc1.1[D11N] and Vc1.1[PeIA], were generated using Modeller based on the NMR structure of Vc1.1(PDB code 2H8S).[38]

Molecular dynamic simulations

The protonation states of His, Asp and Glu residues at the conotoxin/nAChR complexes were predicted using the PropKa 3.1 method.[39] The models were minimized and refined using molecular dynamics (MD) simulations performed with the Amber 16 package and ff14SB force field.[40,41] The receptor complexes were solvated in a truncated octahedral TIP3P water box containing ~10800 water molecules. Sodium ions were added to neutralize the systems. The systems were first minimized with 3,000 steps of steepest descent and then 3,000 steps of conjugate gradient with the solute restrained to their position by a harmonic force of 100 kcal/mol·Å^2. A second minimization was then performed but with all position restraints withdrawn. The systems were then gradually heated up from 50 to 300 K in the NVT ensemble over 100 ps with the solute restrained to their position using a 5 kal/mol·Å^2 harmonic force potential. MD simulations were then carried out in the NPT ensemble, and the position restraints were gradually removed over 100 ps. The production runs were conducted over 50 ns simulation time with pressure coupling set at 1 atm and a constant temperature of 300 K. The MD simulations used a time step of 2 fs and, all bonds involving

hydrogen atoms were maintained to their standard length using the SHAKE algorithm.[42] The particle-mesh Ewald (PME) method was used to model long-range electrostatic interactions.[43] MD trajectories were analyzed using VMD (http://www.ks.uiuc.edu/) and molecules were drawn using PyMol (Schrödinger, LLC).

For validation of the Vc1.1 analogue stability, 100 ns repeated MD simulations were performed on Vc1.1[N9D] and Vc1.1[PeIA] systems respectively, using the same method as described above.

Binding energy decomposition

To quantify the binding energy contribution of these key residues in the ligand binding site, binding energy decomposition was carried out using the MMPBSA.py script in AMBER16.[44] The binding free energy ($\Delta G_{binding}$) values were calculated using the following equation:

$$\Delta G_{binding} = G_{complex} - G_{ligand} - G_{receptor} \quad (1)$$

where the binding free energy ($\Delta G_{binding}$) was determined using MMGB/SA method.[45] This method was identified in our previous study as being slightly more efficient for ranking mutational energies based on homology models than the MMPB/SA method. Details of the MMGB/SA method on peptide binding energy calculation was described in our previous modelling studies.[30]

Thermodynamic mutant cycles

The coupling coefficient (Ω) and coupling energy (ΔG_{couple}) was determined using equations (2) and (3) respectively:

Ω = K_i of wild-type toxin at wild-type channel·K_i of mutant toxin at mutant channel/K_i of wild-type toxin at mutant channel·K_i of mutant toxin at wild-type channel (2) [32]

where K_i = equilibrium inhibition constant (IC_{50})

$$\Delta G_{couple} = -RT\ln(\Omega) \quad (3)$$

where R = gas constant, T = temperature

Peptide synthesis

Procedures for solid peptide synthesis of Vc1.1 analogues were nearly the same as described previously.[24] Briefly, Vc1.1[D11N] and Vc1.1[PeIA] were assembled on rink amide

methylbenzhydrylamine resin (Novabiochem) using solid-phase peptide synthesis with a neutralization/2-(1H-benzotriazol-1-yl)-1,1,3,3-tetramethyluronium hexafluorophosphate activation procedure for Fmoc (*N*-(9-fluorenyl)methoxycarbonyl) chemistry. Cleavage was achieved by treatment with 88:5:5:2 ratio of trifluoroacetic acid (TFA), phenol, water and triisopropylsilane as scavengers, at room temperature (20−25 °C) for 2 h. TFA was evaporated at low pressure in a rotary evaporator. Peptides were precipitated with ice-cold ether, filtered, dissolved in 50% buffer A/B (buffer A consists of 99.95% H_2O/ 0.05% TFA and buffer B consists of 90% CH_3CN/10% H_2O/0.045% TFA), and lyophilized. Crude peptides were purified by RP-HPLC on a Phenomenex C_{18} column, and its molecular mass was confirmed using electrospray mass spectrometry before they were pooled and lyophilized for oxidation. The four cystines in the peptides were selectively oxidized in two steps. In the first step the non-protected cystines were oxidized in 0.1 M NH_4HCO_3 (pH 8–8.5) at a concentration of 0.5 mg/ml, and stirred at room temperature overnight. In the second step, the Acm-protected cystines were oxidized by dissolving the peptides in iodine solution filled at concentration of 1 mg/ml, and stirred for 30 min. Ascorbic acid was then added to stop the oxidizing reaction and the solution was stirred again until no colour was visible. After two rounds of oxidation, peptides were purified by RP-HPLC and their mass (Figure S7) and purity (Figure S8) were validated using electrospray-mass spectrometry (MS) and analytical RP-HPLC, respectively.

Circular dichroism (CD) study

CD spectra were performed on Jasco J-810 spectropolarimeter over the wavelength range of 250-190 nm using a 1.0 mm path length cell, a bandwidth of 1.0 nm, a response time of 2 s, and averaging over three scans. Spectra were recorded at room temperature under nitrogen atmosphere. Peptides were dissolved in buffer A and buffer B. The concentration of Vc1.1, Vc1.1[D11N], Vc1.1[PeIA], and PeIA was 0.28 mM, 0.28 mM, 0.29 mM and 0.30 mM, respectively. The spectra are expressed as molar ellipticity ($[\theta]$)·$[\theta] = 1000 \cdot mdeg/(l \cdot c)$ where, mdeg is the raw CD data, c is the peptide molar concentration (mM), and l is cell path length (mm).

PCR site-directed mutagenesis

N154G mutation to the hα9 nAChR subunit in plasmid pT7TS was done using PrimeSTAR Max kit (Takara Bio, Kusatsu, Shiga, Japan). Mutation was confirmed by DNA sequencing (Australian Genome Research Facility, Melbourne, VIC, Australia).

In vitro cRNA synthesis

Plasmid pT7TS constructs of hα9 and hα10 nAChR subunits were linearized with *XbaI* restriction enzyme (NEB, Ipswich, MA) for *in vitro* cRNA transcription using T7 mMessage mMachine transcription kits (AMBION, Foster City, CA, USA).

Oocyte preparation and microinjection.

All procedures were approved by the University of Sydney Animal Ethics Committee (project number 2016/970). Stage V-VI oocytes (Dumont's classification; 1200-1300 μm diameter) were obtained from *Xenopus laevis*, defolliculated with 1.5 mg/ml collagenase Type II (Worthington Biochemical Corp., Lakewood, NJ) at room temperature for 1-2 h in OR-2 solution containing (in mM) 82.5 NaCl, 2 KCl, 1 $MgCl_2$ and 5 HEPES at pH 7.4. Oocytes were injected with 35 ng cRNA for hα9α10 nAChR (concentration confirmed spectrophotometrically and by gel electrophoresis) at α9:α10 subunit mRNA ratios of 1:1. 1:3 and 3:1, using glass pipettes pulled from glass capillaries (3-000-203 GX, Drummond Scientific Co., Broomall, PA, USA). Oocytes were incubated at 18 ºC in sterile ND96 solution composed of (in mM) 96 NaCl, 2 KCl, 1 $CaCl_2$, 1 $MgCl_2$ and 5 HEPES at pH 7.4, supplemented with 5% FBS, 50 mg/L gentamicin (GIBCO, Grand Island, NY, USA) and 10000 U/mL penicillin-streptomycin (GIBCO, Grand Island, NY, USA).

Oocyte two-electrode voltage clamp recording and data analysis.

Electrophysiological recordings were carried out 2–5 days post cRNA microinjection. Two-electrode voltage clamp recordings of *X. laevis* oocytes expressing human nAChRs were performed at room temperature (21−24 °C) using a GeneClamp 500B amplifier and pClamp9 software interface (Molecular Devices, Sunnyvale, CA, USA) at a holding potential −80 mV. Voltage-recording and current-injecting electrodes were pulled from GC150T-7.5 borosilicate glass (Harvard Apparatus, Holliston, MA) and filled with 3 M KCl giving resistances of 0.3–1 MΩ.

Oocytes were incubated in 100 μM BAPTA-AM ~3 h before recording and perfused with ND115 solution containing (in mM): 115 NaCl, 2.5 KCl, 1.8 $CaCl_2$, and 10 HEPES at pH 7.4 using a continuous Legato 270 push/pull syringe pump perfusion system (KD Scientific, Holliston, MA, USA) at a rate of 2 mL/min in an OPC-1 perfusion chamber of < 20 μL volume (Automate Scientific, Berkeley, CA, USA). Due to the Ca^{2+} permeability of hα9α10 nAChRs, BAPTA-AM incubation was carried out to prevent the activation of *X. laevis* oocyte endogenous Ca^{2+}-activated chloride channels.

Initially, oocytes were briefly washed with ND115 solution followed by 3 applications of acetylcholine (ACh) at a half-maximal excitatory ACh concentration (EC_{50}) for hα9α10 nAChRs. Washout with bath solution was done for 3 min between ACh applications. Oocytes were incubated with peptides for 5 min with the perfusion system turned off, followed by co-application of ACh and peptide with flowing bath solution. All peptide solutions were prepared in ND115 + 0.1 % bovine serum albumin. Peak current amplitudes before (ACh alone) and after (ACh + peptide) peptide incubation were measured using Clampfit version 10.7.0.3 software (Molecular Devices, Sunnyvale, CA, USA), where the ratio of ACh + peptide-evoked current amplitude to ACh alone-evoked current amplitude was used to assess the activity of the peptides at hα9α10 nAChRs. All electrophysiological data were pooled (n = 3-16) and represent means ± standard error of the mean (SEM). Data analysis was performed using GraphPad Prism 5 (GraphPad Software, La Jolla, CA, USA). ACh EC_{50} and α-conotoxin IC_{50} values were determined from concentration-response relationships fitted to a non-linear regression function and reported with error of the fit. Data sets were compared using Tukey's test. Differences were regarded statistically significant when $p < 0.05$.

Supporting Information

Activity of the α-conotoxins at the human α9α10 nAChRs is shown in Figure S1. Internal backbone H-bond between PeIA residues H5 and C8 is shown in Figure S2. Side chain energetic contribution to the α-conotoxin binding affinity is shown in Figure S3. Activities of the α-conotoxins at human

α9α10 and α9[N154G]α10 nAChRs expressed from varied α9:α10 mRNA ratios are shown in Figure S4. Structural comparison of wild-type Vc1.1 and analogues Vc1.1[D11N] and Vc1.1[PeIA] from MD simulations are shown in Figure S5. Circular dichroism spectra of Vc1.1, Vc1.1[D11N], Vc1.1[PeIA] and PeIA are shown in Figure S6. MS and analytical HPLC spectra of Vc1.1, Vc1.1[D11N], Vc1.1[PeIA], PeIA and RgIA# are shown in Figure S7 and Figure S8, respectively.

Corresponding Author Information

*E-mail: ryu@ouc.edu.cn

*E-mail: djadams@uow.edu.au (**ORCID iD:** 0000-0002-7030-2288)

Author Contributions

†(R.Y, H-S.T.) These authors contributed equally to this work. R.Y. performed computational modeling, analyzed the data, and contributed to writing the paper; H-S.T. conducted the electrophysiological experiments, analyzed the data and contributed to writing the paper; N.T. J. S. and T. J. conducted peptide synthesis; D.J.A., R.Y. and H-S.T. conceived the idea of the project, provided the financial support and resources, and contributed to writing the paper.

Notes

The authors declare no competing financial interest.

Acknowledgments

This work was supported by the grant from National Natural Science Foundation of China (NSFC) (No. 81502977 for R.Y.), the Fundamental Research Funds for the Central Universities (No. 201512007,201762011 for R.Y.), Innovation Project from Qingdao National Laboratory for Marine Science and Technology (No. 2015ASKJ02), the NSFC-Shandong Joint Fund (No. U1406402) and the Australian Research Council (Discovery Project Grant DP150103990 for D.J.A.).

Abbreviations Used

nAChR, nicotinic acetylcholine receptor; AChBP, acetylcholine binding protein; HBTU, neutralization/2-(1H-benzotriazol-1-yl)-1,1,3,3-tetramethyluronium hexafluorophosphate; MBHA; rink amide methylbenzhydrylamine; MD, molecular dynamics; RP-HPLC, reversed-phase HPLC;

Vc1.1, α-conotoxin Vc1.1; PeIA, α-conotoxin PeIA; RgIA#, α-conotoxin RgIA with the R13 truncated and C-termini amidation; Vc1.1[D11N], α-conotoxin Vc1.1 [D11N] mutant; Vc1.1[PeIA], α-conotoxin Vc1.1 grafted with residues from the second loop of PeIA; RMSD, root mean square deviation; EC_{50}, half-maximal excitatory concentration; IC_{50}, half-maximal inhibitory concentration.

Homology models

Authors will release the atomic coordinates and experimental data upon article publication.

References

(1) Changeux, J.-P. The Nicotinic Acetylcholine Receptor: The Founding Father of the Pentameric Ligand-Gated Ion Channel Superfamily. *J. Biol. Chem.* **2012**, *287* (48), 40207–40215.

(2) Taly, A.; Corringer, P.-J.; Guedin, D.; Lestage, P.; Changeux, J.-P. Nicotinic Receptors: Allosteric Transitions and Therapeutic Targets in the Nervous System. *Nat. Rev. Drug Discov.* **2009**, *8* (9), 733–750.

(3) Morales-Perez, C. L.; Noviello, C. M.; Hibbs, R. E. X-Ray Structure of the Human A4β2 Nicotinic Receptor. *Nature* **2016**, *538* (7625), 411–415.

(4) Vetter, D. E.; Katz, E.; Maison, S. F.; Taranda, J.; Turcan, S.; Ballestero, J.; Liberman, M. C.; Elgoyhen, A. B.; Boulter, J. The α10 Nicotinic Acetylcholine Receptor Subunit Is Required for Normal Synaptic Function and Integrity of the Olivocochlear System. *Proc. Natl. Acad. Sci. U. S. A.* **2007**, *104* (51), 20594–20599.

(5) Morley, B. J.; Lysakowski, A.; Vijayakumar, S.; Menapace, D.; Jones, T. A. Nicotinic Acetylcholine Receptors Regulate Vestibular Afferent Gain and Activation Timing. *J. Comp. Neurol.* **2017**, *525* (5), 1216–1233.

(6) Lips, K. S.; Pfeil, U.; Kummer, W. Coexpression of Alpha 9 and Alpha 10 Nicotinic Acetylcholine Receptors in Rat Dorsal Root Ganglion Neurons. *Neuroscience* **2002**, *115* (1), 1–5.

(7) Hone, A. J.; Servent, D.; McIntosh, J. M. α9-Containing Nicotinic Acetylcholine Receptors and the Modulation of Pain. *Br. J. Pharmacol.* **2017**.

(8) Colomer, C.; Olivos-Oré, L. A.; Vincent, A.; McIntosh, J. M.; Artalejo, A. R.; Guérineau, N. C. Functional Characterization of α9-Containing Cholinergic Nicotinic Receptors in the Rat Adrenal Medulla: Implication in Stress-Induced Functional Plasticity. *J. Neurosci. Off. J. Soc. Neurosci.* **2010**, *30* (19), 6732–6742.

(9) Nguyen, V. T.; Ndoye, A.; Grando, S. A. Novel Human α9 Acetylcholine Receptor Regulating Keratinocyte Adhesion Is Targeted by Pemphigus Vulgaris Autoimmunity. *Am. J. Pathol.* **2000**, *157* (4), 1377–1391.

(10) Sgard, F.; Charpantier, E.; Bertrand, S.; Walker, N.; Caput, D.; Graham, D.; Bertrand, D.; Besnard, F. A Novel Human Nicotinic Receptor Subunit, α10, That Confers Functionality to the α9-Subunit. *Mol. Pharmacol.* **2002**, *61* (1), 150–159.

(11) Chernyavsky, A.; Chen, Y.; Wang, P. H.; Grando, S. A. Pemphigus Vulgaris Antibodies Target the Mitochondrial Nicotinic Acetylcholine Receptors That Protect Keratinocytes from Apoptolysis. *Int. Immunopharmacol.* **2015**, *29* (1), 76–80.

(12) Peng, H.; Ferris, R. L.; Matthews, T.; Hiel, H.; Lopez-Albaitero, A.; Lustig, L. R. Characterization of the Human Nicotinic Acetylcholine Receptor Subunit alpha (α) 9 (CHRNA9) and alpha (α) 10 (CHRNA10) in Lymphocytes. *Life Sci.* **2004**, *76* (3), 263–280.

(13) Koval, L.; Lykhmus, O.; Zhmak, M.; Khruschov, A.; Tsetlin, V.; Magrini, E.; Viola, A.; Chernyavsky, A.; Qian, J.; Grando, S.; Komisarenko, S.; Skok, M. Differential Involvement of α4β2, α7 and α9α10 Nicotinic Acetylcholine Receptors in B Lymphocyte Activation in Vitro. *Int. J. Biochem. Cell Biol.* **2011**, *43* (4), 516–524.

(14) Mikulski, Z.; Hartmann, P.; Jositsch, G.; Zasłona, Z.; Lips, K. S.; Pfeil, U.; Kurzen, H.; Lohmeyer, J.; Clauss, W. G.; Grau, V.; Fronius, M.; Kummer, W. Nicotinic Receptors on Rat Alveolar Macrophages Dampen ATP-Induced Increase in Cytosolic Calcium Concentration. *Respir. Res.* **2010**, *11*, 133.

(15) Zarghooni, S.; Wunsch, J.; Bodenbenner, M.; Brüggmann, D.; Grando, S. A.; Schwantes, U.; Wess, J.; Kummer, W.; Lips, K. S. Expression of Muscarinic and Nicotinic Acetylcholine Receptors in the Mouse Urothelium. *Life Sci.* **2007**, *80* (24–25), 2308–2313.

(16) Romero, H. K.; Christensen, S. B.; Di Cesare Mannelli, L.; Gajewiak, J.; Ramachandra, R.; Elmslie, K. S.; Vetter, D. E.; Ghelardini, C.; Iadonato, S. P.; Mercado, J. L.; Olivera, B. M.; McIntosh, J. M. Inhibition of α9α10 Nicotinic Acetylcholine Receptors Prevents Chemotherapy-Induced Neuropathic Pain. *Proc. Natl. Acad. Sci. U. S. A.* **2017**, *114* (10), E1825–

E1832.
(17) Mohammadi, S.; Christie, M. J. α9-Nicotinic Acetylcholine Receptors Contribute to the Maintenance of Chronic Mechanical Hyperalgesia, but Not Thermal or Mechanical Allodynia. *Mol. Pain* **2014**, *10*, 64.
(18) Lee, C.-H.; Huang, C.-S.; Chen, C.-S.; Tu, S.-H.; Wang, Y.-J.; Chang, Y.-J.; Tam, K.-W.; Wei, P.-L.; Cheng, T.-C.; Chu, J.-S.; Chen, L.-C.; Wu, C.-H.; Ho, Y.-S. Overexpression and Activation of the α9-Nicotinic Receptor during Tumorigenesis in Human Breast Epithelial Cells. *J. Natl. Cancer Inst.* **2010**, *102* (17), 1322–1335.
(19) Vincler, M.; Wittenauer, S.; Parker, R.; Ellison, M.; Olivera, B. M.; McIntosh, J. M. Molecular Mechanism for Analgesia Involving Specific Antagonism of α9α10 Nicotinic Acetylcholine Receptors. *Proc. Natl. Acad. Sci. U. S. A.* **2006**, *103* (47), 17880–17884.
(20) Luo, S.; Zhangsun, D.; Harvey, P. J.; Kaas, Q.; Wu, Y.; Zhu, X.; Hu, Y.; Li, X.; Tsetlin, V. I.; Christensen, S.; Romero, H. K.; McIntyre, M.; Dowell, C.; Baxter, J. C.; Elmslie, K. S.; Craik, D. J.; McIntosh, J. M. Cloning, Synthesis, and Characterization of αO-Conotoxin GeXIVA, a Potent α9α10 Nicotinic Acetylcholine Receptor Antagonist. *Proc. Natl. Acad. Sci. U. S. A.* **2015**, *112* (30), E4026-4035.
(21) McIntosh, J. M.; Plazas, P. V.; Watkins, M.; Gomez-Casati, M. E.; Olivera, B. M.; Elgoyhen, A. B. A Novel α-Conotoxin, PeIA, Cloned from *Conus Pergrandis*, Discriminates between Rat α9α10 and α7 Nicotinic Cholinergic Receptors. *J. Biol. Chem.* **2005**, *280* (34), 30107–30112.
(22) Daly, N. L.; Callaghan, B.; Clark, R. J.; Nevin, S. T.; Adams, D. J.; Craik, D. J. Structure and Activity of α-Conotoxin PeIA at Nicotinic Acetylcholine Receptor Subtypes and GABA(B) Receptor-Coupled N-Type Calcium Channels. *J. Biol. Chem.* **2011**, *286* (12), 10233–10237.
(23) Plazas, P. V.; Katz, E.; Gomez-Casati, M. E.; Bouzat, C.; Elgoyhen, A. B. Stoichiometry of the α9α10 Nicotinic Cholinergic Receptor. *J. Neurosci. Off. J. Soc. Neurosci.* **2005**, *25* (47), 10905–10912.
(24) Yu, R.; Kompella, S. N.; Adams, D. J.; Craik, D. J.; Kaas, Q. Determination of the α-Conotoxin Vc1.1 Binding Site on the α9α10 Nicotinic Acetylcholine Receptor. *J. Med. Chem.* **2013**, *56* (9), 3557–3567.
(25) Indurthi, D. C.; Pera, E.; Kim, H.-L.; Chu, C.; McLeod, M. D.; McIntosh, J. M.; Absalom, N. L.; Chebib, M. Presence of Multiple Binding Sites on α9α10 NAChR Receptors Alludes to Stoichiometric-Dependent Action of the α-Conotoxin, Vc1.1. *Biochem. Pharmacol.* **2014**, *89* (1), 131–140.
(26) Azam, L.; Papakyriakou, A.; Zouridakis, M.; Giastas, P.; Tzartos, S. J.; McIntosh, J. M. Molecular Interaction of α-Conotoxin RgIA with the Rat α9α10 Nicotinic Acetylcholine Receptor. *Mol. Pharmacol.* **2015**, *87* (5), 855–864.
(27) Halai, R.; Callaghan, B.; Daly, N. L.; Clark, R. J.; Adams, D. J.; Craik, D. J. Effects of Cyclization on Stability, Structure, and Activity of α-Conotoxin RgIA at the α9α10 Nicotinic Acetylcholine Receptor and GABA(B) Receptor. *J. Med. Chem.* **2011**, *54* (19), 6984–6992.
(28) Ellison, M.; Feng, Z.-P.; Park, A. J.; Zhang, X.; Olivera, B. M.; McIntosh, J. M.; Norton, R. S. α-RgIA, a Novel Conotoxin That Blocks the α9α10 NAChR: Structure and Identification of Key Receptor-Binding Residues. *J. Mol. Biol.* **2008**, *377* (4), 1216–1227.
(29) Quiram, P. A.; Jones, J. J.; Sine, S. M. Pairwise Interactions between Neuronal α7 Acetylcholine Receptors and α-Conotoxin ImI. *J. Biol. Chem.* **1999**, *274* (28), 19517–19524.
(30) Yu, R.; Craik, D. J.; Kaas, Q. Blockade of Neuronal α7-NAChR by α-Conotoxin ImI Explained by Computational Scanning and Energy Calculations. *PLoS Comput. Biol.* **2011**, *7* (3), e1002011.
(31) Halai, R.; Clark, R. J.; Nevin, S. T.; Jensen, J. E.; Adams, D. J.; Craik, D. J. Scanning Mutagenesis of α-Conotoxin Vc1.1 Reveals Residues Crucial for Activity at the α9α10 Nicotinic Acetylcholine Receptor. *J. Biol. Chem.* **2009**, *284* (30), 20275–20284.
(32) Hidalgo, P.; MacKinnon, R. Revealing the Architecture of a K^+ Channel Pore through Mutant Cycles with a Peptide Inhibitor. *Science* **1995**, *268* (5208), 307–310.

(33) Markovitch, O.; Agmon, N. Structure and Energetics of the Hydronium Hydration Shells. *J. Phys. Chem. A* **2007**, *111* (12), 2253–2256.
(34) Boffi, J. C.; Marcovich, I.; Gill-Thind, J. K.; Corradi, J.; Collins, T.; Lipovsek, M. M.; Moglie, M.; Plazas, P. V.; Craig, P. O.; Millar, N. S.; Bouzat, C.; Elgoyhen, A. B. Differential Contribution of Subunit Interfaces to α9α10 Nicotinic Acetylcholine Receptor Function. *Mol. Pharmacol.* **2017**, *91* (3), 250–262.
(35) Magrane, M.; UniProt Consortium. UniProt Knowledgebase: A Hub of Integrated Protein Data. *Database J. Biol. Databases Curation* **2011**, *2011*, bar009.
(36) Zouridakis, M.; Giastas, P.; Zarkadas, E.; Chroni-Tzartou, D.; Bregestovski, P.; Tzartos, S. J. Crystal Structures of Free and Antagonist-Bound States of Human α9 Nicotinic Receptor Extracellular Domain. *Nat. Struct. Mol. Biol.* **2014**, *21* (11), 976–980.
(37) Celie, P. H. N.; Kasheverov, I. E.; Mordvintsev, D. Y.; Hogg, R. C.; van Nierop, P.; van Elk, R.; van Rossum-Fikkert, S. E.; Zhmak, M. N.; Bertrand, D.; Tsetlin, V.; Sixma, T. K.; Smit, A. B. Crystal Structure of Nicotinic Acetylcholine Receptor Homolog AChBP in Complex with an α-Conotoxin PnIA Variant. *Nat. Struct. Mol. Biol.* **2005**, *12* (7), 582–588.
(38) Clark, R. J.; Fischer, H.; Nevin, S. T.; Adams, D. J.; Craik, D. J. The Synthesis, Structural Characterization, and Receptor Specificity of the α-Conotoxin Vc1.1. *J. Biol. Chem.* **2006**, *281* (32), 23254–23263.
(39) Olsson, M. H. M.; Søndergaard, C. R.; Rostkowski, M.; Jensen, J. H. PROPKA3: Consistent Treatment of Internal and Surface Residues in Empirical PKa Predictions. *J. Chem. Theory Comput.* **2011**, *7* (2), 525–537.
(40) Maier, J. A.; Martinez, C.; Kasavajhala, K.; Wickstrom, L.; Hauser, K. E.; Simmerling, C. Ff14SB: Improving the Accuracy of Protein Side Chain and Backbone Parameters from Ff99SB. *J. Chem. Theory Comput.* **2015**, *11* (8), 3696–3713.
(41) Case, D.A.; Cerutti, D.S.; Cheatham, T.E.;, Darden, III, T.A.; Duke, R.E.; Giese, T.J.; Gohlke, H.; Goetz, A.W.; Greene, D.; Homeyer, N.; Izadi, S.; Kovalenko, A.; Lee, T.S.; LeGrand, S.; Li, P.; Lin, C.; Liu, J.; Luchko, T.; Luo, R.; Mermelstein, D.; Merz, K.M.; Monard, G.; Nguyen, H.; Omelyan, I.; Onufriev, A.; Pan, F.; Qi, R.; Roe, D.R.; Roitberg, A.; Sagui, C.; Simmerling, C.L.; Botello-Smith, W.M.; Swails, J.; Walker, R.C.; Wang, J.; Wolf, R.M.; Wu, X.; Xiao, L.; York D.M., and Kollman, P.A. AMBER 2017, University of California, San Francisco: San Francisco, CA, 2017.
(42) Miyamoto, S.; Kollman, P. A. Settle: An Analytical Version of the SHAKE and RATTLE Algorithm for Rigid Water Models. *J. Comput. Chem.* **1992**, *13* (8), 952–962.
(43) Darden, T.; York, D.; Pedersen, L. J. Particle mesh Ewald: An N · log(N) method for Ewald sums in large systems. Chem. Phys. 1993, 98, 10089–10092.
(44) Miller, B. R.; McGee, T. D.; Swails, J. M.; Homeyer, N.; Gohlke, H.; Roitberg, A. E. MMPBSA.Py: An Efficient Program for End-State Free Energy Calculations. *J. Chem. Theory Comput.* **2012**, *8* (9), 3314–3321.
(45) Onufriev, A.; Bashford, D.; Case, D. A. Exploring Protein Native States and Large-Scale Conformational Changes with a Modified Generalized Born Model. *Proteins* **2004**, *55* (2), 383–394.

Table 1. **Inhibition of hα9α10 and hα9[N154]α10 expressed from α9/α9[N154G]:α10 mRNA injection ratios of 1:3 and 3:1 by Vc1.1 and analogues.**

Receptor	α9:α10	ACh (μM)	Vc1.1 (μM)	Vc1.1[D11N] (μM)	Vc1.1[PeIA] (μM)
hα9α10	1:3	47.42 ± 5.77	3.57 ± 0.31	17.54 ± 2.11	13.23 ± 1.80
	3:1	40.00 ± 5.98	0.75 ± 0.09	10.79 ± 1.14	9.30 ± 0.86
hα9[N154G]α10	1:3	13.12 ± 0.93	11.25 ± 1.50	10.24 ± 0.69	12.96 ± 1.89
	3:1	34.28 ± 3.99	17.02 ± 3.17	8.59 ± 0.77	15.2 ± 1.34

EC_{50} values (mean ± error of the fit, n = 3-4) obtained from the fit of the ACh concentration-response relationship for hα9α10 and hα9[N154G]α10 nAChRs expressed from α9/α9[N154G]:α10 mRNA injection ratios of 1:3 and 3:1

IC_{50} values (mean ± error of the fit, n = 3-16) obtained from the fit of the concentration-response relationships for the inhibition of hα9α10 and hα9[N154G]α10 nAChRs expressed from α9/α9[N154G]:α10 mRNA injection ratios of 1:3 and 3:1 by Vc1.1, Vc1.1[D11N], and Vc1.1[PeIA].

Figures

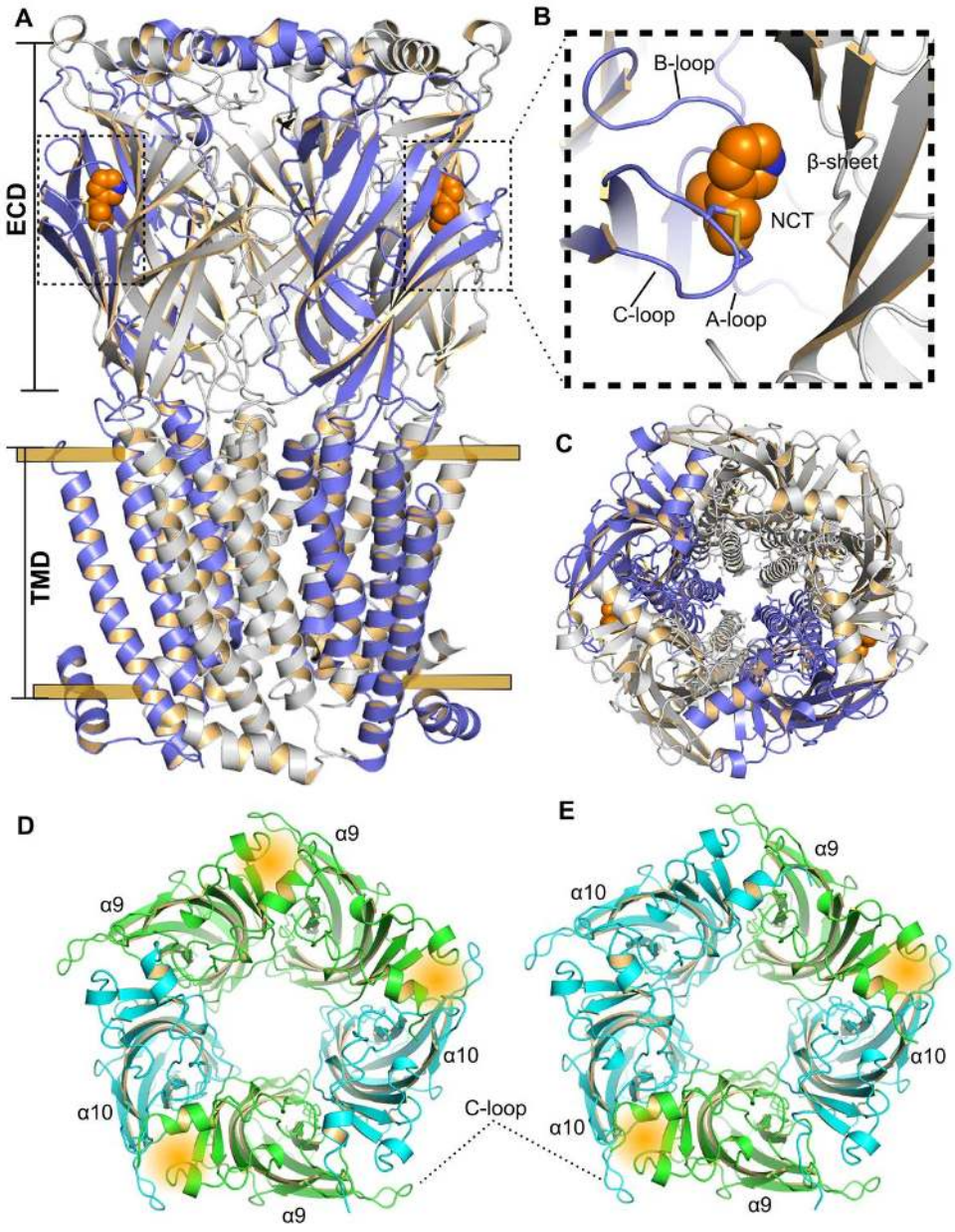
A
ECD
TMD
B
B-loop
β-sheet
NCT
C-loop
A-loop
C
D
α9
α9
α10
α10
C-loop
α9
E
α9
α10
α10
α10
α9

Figure 1. Structures of the nAChRs. (A) Side view of the human α4β2 nAChR crystal structure showing the extracellular (ECD) and transmembrane (TMD) domains. Two nicotine molecules (NCT, orange) are bound to the ECD binding site (dashed frame) (PDB code: 5KXI). The α4 and β2 subunits are colored blue and grey, respectively. (B) The ligand binding site magnified (dashed frame) comprising of loops A, B and C of the α4 subunit (principal component (+)) and β-sheet of the β4 subunit (complementary component (−)); (C) Top view of the human α4β2 nAChR; (D,E) Top view of the $(\alpha9)_2(\alpha10)_3$ nAChR and $(\alpha9)_3(\alpha10)_2$ nAChR homology models, respectively. The α-conotoxin binding site is located at the cleft between the α10(+) and α9(−) components or α9(+) and α9(−) components (orange cloud). The (+) component contributes the C-loop to the binding site, and the (−) component contributes the β-sheet to the binding pocket. These models were built using multiple templates, including the crystal structures of *Aplysia californica* AChBP (PDB code: 2BR8) and the human α9 nAChR subunit ECD (PDB code: 4UY2).

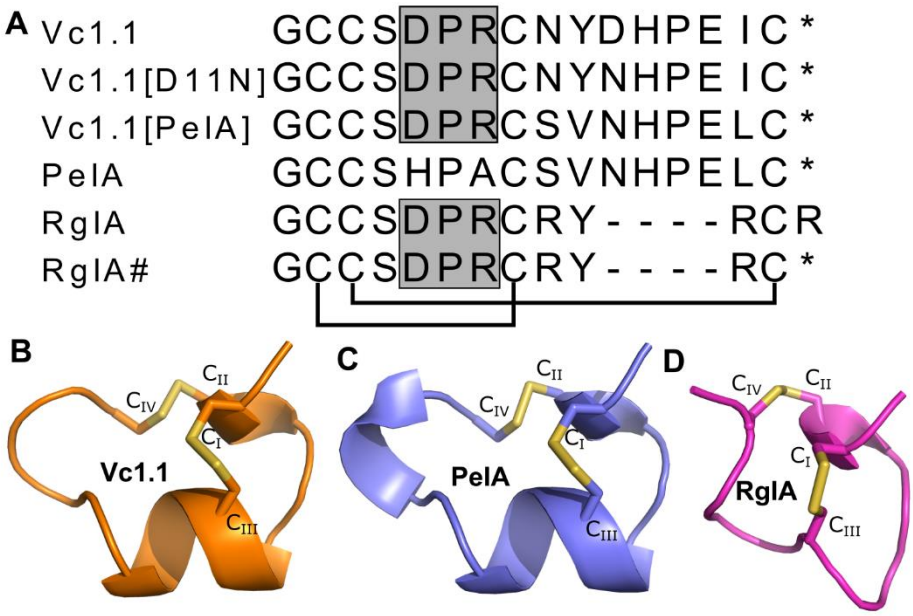

Figure 2: Sequence alignment and structures of the α-conotoxins. (A) Sequence alignment of the α-conotoxin Vc1.1, PeIA, RgIA# and their analogues. There are two disulphide bonds (black lines) linking C_I and C_{III}, and C_{II} and C_{IV}, respectively. The DPR motif is highlighted using the grey background. Vc1.1 and PeIA possess a 4/7 disulphide framework, and RgIA has a 4/3 disulphide framework. * represents the amide group of the C-termini. (B) and (D) NMR structures of Vc1.1 (PDB code: 2H8S) and RgIA (PDB code: 2JUT), and (C) crystal structure of PeIA (PDB code: 5JME).

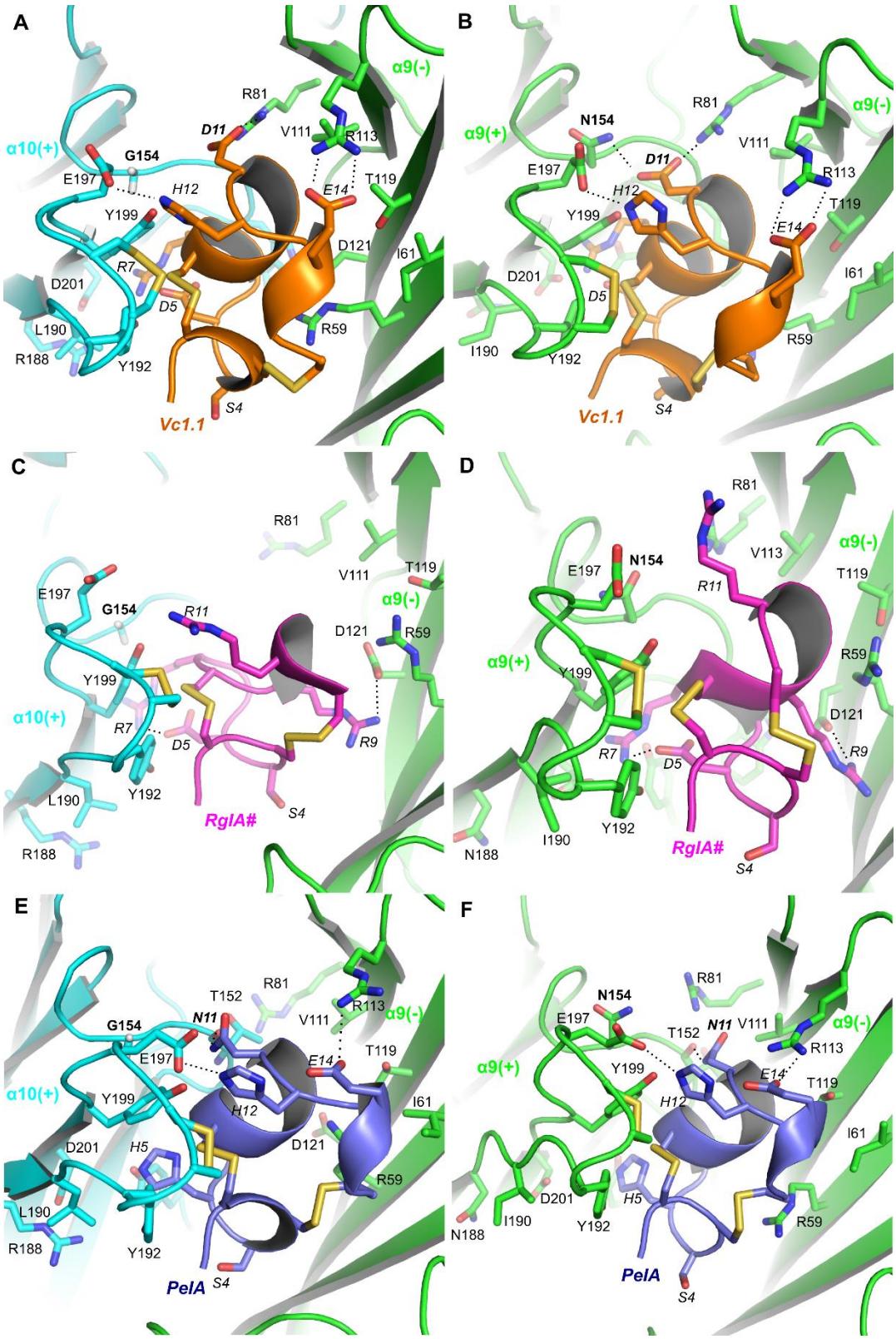
A
α9(-)
R81
D11
V111
R113
α10(+)
G154
E197
H12
E14
T119
Y199
D121
I61
R7
D201
D5
R59
L190
R188
Y192
S4
Vc1.1
B
α9(+)
N154
R81
α9(-)
E197
D11
V111
R113
H12
T119
Y199
E14
D201
D5
I61
I190
R59
Y192
S4
Vc1.1
C
R81
V111
T119
E197
G154
R11
α9(-)
D121
R59
Y199
α10(+)
R7
D5
R9
L190
Y192
RglA#
S4
R188
D
R81
N154
V113
α9(-)
E197
R11
T119
α9(+)
Y199
R59
D121
R7
D5
R9
I190
Y192
N188
RglA#
S4
E
T152
R81
R113
α9(-)
G154
N11
V111
E197
E14
T119
α10(+)
Y199
H12
I61
D201
H5
D121
R59
L190
R188
Y192
PelA
S4
F
R81
N154
E197
T152
N11
V111
α9(-)
R113
α9(+)
Y199
E14
T119
H12
I61
D201
H5
I190
R59
N188
Y192
PelA
S4

Figure 3. Binding of the α-conotoxins at the human α10(+)-α9(−) and α9(+)-α9(−) interfaces. (A,B), (C,D), and (E,F) α-Conotoxins Vc1.1, RgIA# and PeIA bound to the interfaces of α10(+)-α9(—) (left panels) and α9(+)-α9(—) (right panels), respectively. The α10 and α9 subunits are shown in cyan and green, respectively. Dashed lines indicate hydrogen bonds formed between the α-conotoxins and α9α10 nAChR.

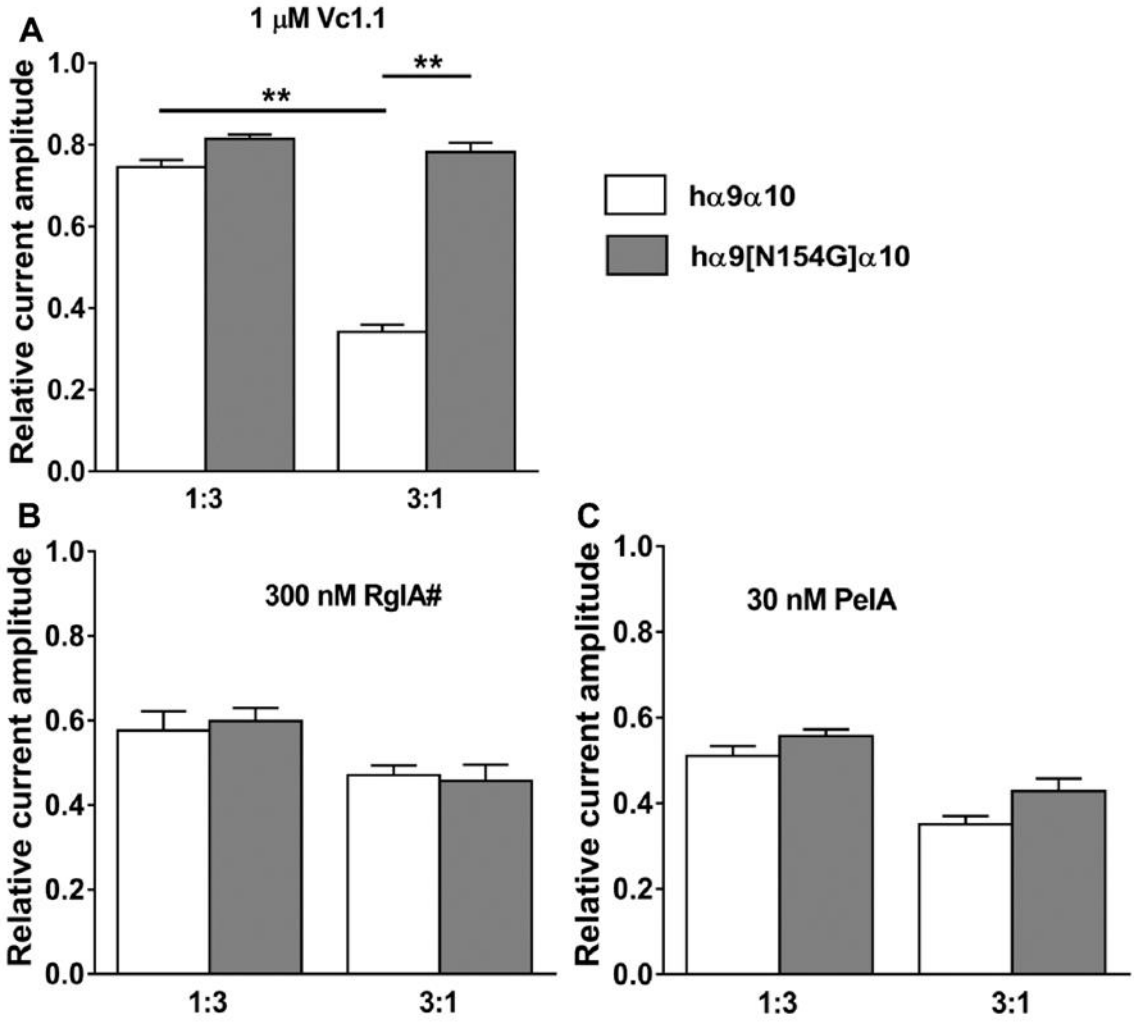

Figure 4. Activity of the α-conotoxins at human α9α10 and α9[N154G]α10 nAChRs expressed from varied α9:α10 mRNA ratios. Bar graphs of relative ACh-evoked current amplitude mediated by hα9α10 and hα9[N154G]α10 nAChRs in the presence of (A) 1 μM Vc1.1, (B) 300 nM RgIA#, and (C) 30 nM PeIA. Whole-cell hα9α10 nAChR-mediated currents at 1:3 and 3:1 ratios were activated by 50 μM and 30 μM ACh, respectively, and hα9[N154G]α10 nAChR-mediated currents at 1:3 and 3:1 ratios were activated by 20 μM and 30 μM ACh, respectively (close to their respective EC_{50} values). ** $p < 0.0001$